Soft Matter

RSC Publishing

PAPER

Myosin II does it all: assembly, remodeling, and disassembly of actin networks are governed by myosin II activity†

Cite this: *Soft Matter*, 2013, **9**, 7127

Yaron Ideses,[a] Adar Sonn-Segev,[b] Yael Roichman[b] and Anne Bernheim-Groswasser*[a]

Eukaryotic cells rely on their cytoskeleton to carry out coordinated motion, to transport materials within them, and to interact mechanically with their environment. To adapt to the changing requirements, the cell's cytoskeleton constantly remodels through the action of myosin II motor clusters that interact with numerous actin filaments simultaneously. Here we study the various roles of myosin II clusters in the formation and evolution of *in vitro* actomyosin networks as a model system for the cell's cytoskeleton. In our experiments the motor clusters can vary in size between 14 and 144 myosin II molecules and apply forces ranging from several to tens of piconewtons. During the initial process of network formation the motor clusters become embedded within the network structure, where they act as internal active cross-linkers. Myosin II clusters enhance the nucleation of network filaments/bundles in a concentration dependent manner, in the presence of the passive bundling protein fascin, thus functioning as a '*network co-nucleator*'. As network formation is achieved, myosin II turns into a '*network reorganizer*', where it takes part in remodeling and coarsening of the overall network structure. As a result of the strong confinement (the motor clusters within the network bundles exhibit high processivity with a fraction of attached motors $p_{att} \geq 0.15$), their effect on the nucleation and reorganization of the actin network is enhanced, rendering even small clusters of 14 myosin II molecules efficient. The stresses building-up in the networks lead to complex dynamics and can drive their contraction and rupture, depending on the motor concentration and cluster size. Above a certain concentration, the severing and disassembly properties of the motors dominate, and they function as '*network disassembly agents*'. Myosin II motors are shown to be unique motors that function as complex machines that can perform a diversity of tasks, thereby regulating the nature of the assembled network and facilitating its formation.

Received 29th January 2013
Accepted 10th May 2013

DOI: 10.1039/c3sm50309g

www.rsc.org/softmatter

Introduction

The cell cytoskeleton is a spatially extended *active* network, which forms *via* multi-scale self-organization of polar filaments, accessory proteins and molecular motors. Its activity is driven by ATP hydrolysis in processes such as filament polymerization/depolymerization[1] and generation of relative movement between filaments by motor proteins.[2] One special class of molecular motors is myosin II. These motors apply contractile stresses at the molecular level and play a major role in cell adhesion and migration,[3] cell division,[4–6] tissue morphogenesis,[7,8] and polarizing cortical flows.[9,10] A single myosin II motor head does not stay in contact with its actin track throughout its motion; it is inherently non-processive. However, when assembled into large bipolar filaments[11] at least one myosin molecule remains in contact with the actin track at a given instant, such that the overall myosin/actin connection does not break resulting in processive motion towards the plus ends of actin filaments.

The role of myosin II cluster size and processivity on cytoskeletal network reorganization has not been investigated, and its regulation *in vivo* is not fully understood. Yet, it is expected to have a large impact on network elasticity, dynamics, and architecture, since it not only determines the number of filaments/bundles which can simultaneously attach to the same motor aggregate, but also defines the magnitude of forces generated per cluster and the elastic stresses that can develop within the network. Besides serving as an active cross-linker, myosin II motors can actively depolymerize actin filaments,[12] thereby regulating actin turnover by increasing the reservoir of actin monomers available for network polymerization.[13] Myosin II was also shown to function in the turnover of actin during cytokinesis, suggesting that there might be a coupling between the

[a]*Department of Chemical Engineering, Ilse Kats Institute for Nanoscale Science and Technology, Ben Gurion University of the Negev, Beer-Sheva 84105, Israel. E-mail: bernheim@bgu.ac.il*

[b]*School of Chemistry, The Sackler Faculty of Exact Sciences Tel Aviv University, Tel Aviv 69978, Israel*

† Electronic supplementary information (ESI) available. See DOI: 10.1039/c3sm50309g

contractile forces applied by the motors during ring constriction to the rate of actin disassembly.[14–17] Recent evidence for such a coupling was also demonstrated *in vitro*.[18] Despite the increasing evidence that myosin II plays a role in actin turnover, the exact mechanism by which these motors function in filament disassembly is not well understood. It is not clear whether they inhibit filament assembly by accumulating at the plus end of actin filaments, whether they enhance filaments' disassembly by inducing conformational change in the actin filament, or whether they actively disassemble actin subunits during their motion from the minus end towards the filaments' plus end.

To identify the biophysical processes underlying cytoskeletal organization, different *in vitro* model systems of purified motors and filaments have been recently developed. It has been shown that small processive clusters of kinesins can organize microtubules (MT) into asters, vortices, or bundles, depending on the motor concentration.[19–22] The same patterns form whether tubulin or taxol-stabilized MT are used, suggesting that kinesin clusters do not function in the dynamics of polymerization/depolymerization of MT, but serve only as active reorganizing centers for the MT. The development of asters, vortices, and bundles is also observed numerically in numerous theoretical models and computer simulations studying motor-filament systems.[23–32] These theoretical studies also suggest that steady-state patterns are generic and therefore should be experimentally observable in any motor/filament system. Yet, while asters and bundles do form in solutions of myosin II-actin systems, the proposed models do not reproduce many of the patterns and dynamics that are generated in the experiments.[33,34] This discrepancy may originate from the nature of the myosin II motor itself (highly non-processive), from the size of the myosin cluster (which must be large due to the low processivity of individual myosin II motors), from the coupling between actin filaments' disassembly dynamics and myosin II activity, or from the difference in mechanical properties of MT and actin filaments. In comparison to MT, actin filaments have a highly asymmetric load response, *i.e.*, support large tensions but buckle easily under piconewton (pN) compressive loads.[34–36]

Reconstitution of actomyosin network dynamics requires the use of actin monomers (G-actin) as a starting point for *in vitro* network formation[33] in order to reflect faithfully the tight interplay between actin polymerization/depolymerization dynamics and myosin II motors' contractile and reorganization activity. In contrast to the MT/kinesin system,[19–22] the addition of a passive crosslinker is necessary for actomyosin networks to form;[12,33] in its absence the severing and disassembly activity of myosin II dominates and no networks form.[12,33] In this paper we study the various roles of myosin II clusters in the formation and evolution of *in vitro* actomyosin networks as a model system for the cell's cytoskeleton. Using *in vitro* reconstituted networks consisting of actin, myosin II, and the bundling protein fascin[37] we are able to demonstrate that myosin II motor aggregates are embedded inside the actin network from the very initial states of its formation and participate, together with fascin, in the process of network nucleation. We describe the various functionalities of myosin II motors and relate them to the final network morphology and network evolution dynamics. We focus specifically on the effect of myosin II cluster size and concentrations on network formation and reorganization processes.

Materials and methods

Materials

Protein purification. G-actin was purified from rabbit skeletal muscle acetone powder,[38] with a gel filtration step, stored on ice and used within two weeks. Actin was labeled on Cys374 with Alexa-Fluor 488 (Invitrogen). Purification of myosin II skeletal muscle was done according to standard protocols.[39] Myosin II was labeled by modification of the method of Quinlan *et al.*[40] Chicken gizzard RLC mutant A (kind gift from Prof. Yale Goldman, University of Pennsylvania) was labeled with Cy3-maleimide at pairs of engineered cysteine residues. The labeled RLC was exchanged for the endogenous RLC subunits at 6-fold molar excess (RLC/myosin molecule). We did not separate labeled myosin II from free RLC to (i) reduce the time of motor manipulation and thus prevent their degradation (causes inactive or partially active motors) and (ii) in order to prevent contamination of actin and nucleotides (*e.g.*, ATP and ADP) in the final solution (needed for the separation process).[40] This procedure did not cause any deterioration of image processing as the fluorescent signal emanating from individual motor clusters is much larger than the fluorescent signal emanating from free RLC molecules. Recombinant GST–fascin was prepared by a modification of the method of Ono *et al.*[37] The concentration of the various proteins used was determined by absorbance measured using a UV/Visible spectrophotometer (Ultraspec 2100 pro, Pharmacia) in a cuvette with a 1 cm path length using the following extinction coefficients: G-actin ($\varepsilon_{290} = 26\,460\ M^{-1}\ cm^{-1}$), GST–fascin ($\varepsilon_{280} = 99\,330\ M^{-1}\ cm^{-1}$), myosin II dimer ($\varepsilon_{280} = 268\,800\ M^{-1}\ cm^{-1}$), and RLC mutant A ($\varepsilon_{280} = 3960\ M^{-1}\ cm^{-1}$).

Experimental procedure. The *motility medium* contains 10 mM HEPES, pH = 7.0, 1 mM $MgCl_2$, an ATP regenerating system (0.5 mg mL^{-1} creatine kinase and 5 mM creatine phosphate), 200 μM EGTA, an anti-bleaching solution (0.1 mg mL^{-1} glucose oxidase, 0.018 mg mL^{-1} catalase, and 5 mg mL^{-1} glucose), and various amounts of KCl, Mg-ATP, G-actin, myosin II, and fascin. The activity of labeled and unlabeled myosin II motors is similar, and they were used at various ratios 0–100% (labeled/unlabeled).

Network formation. First, myosin II aggregates are prepared by bringing the stock motor solution (at 0.5 M KCl) to the final KCl concentration used in the experiment. Actomyosin network formation is initiated by transferring the preformed motor aggregates into the *motility medium* (see above). 4 μL of that solution was placed between a glass slide and a glass coverslip and sealed with grease. To prevent protein adsorption, the glass coverslip and slide were coated with an inert polymer (PEG-mal $M_w = 5000\ g\ mol^{-1}$ (Nanocs)).

Methods

Cryo-transmission electron microscopy. Specimens for cryo-TEM were prepared in a controlled environment vitrification chamber. All solutions were quenched from 23 °C and 100%

relative humidity. 3 μl of solution was deposited on a holey carbon film TEM grid (lacey carbon, 300 mesh grids, Ted Pella), blotted, and plunged into liquid ethane at its freezing point. Samples are stored under liquid nitrogen before transfer to a TEM (Tecnai 12, FEI) operating at 120 kV in low-dose mode, with underfocus of a few micrometers to increase phase contrast. Images were recorded on a Gatan 794 or Gatan 791 CCD camera with Digital Micrograph software, and analyzed using METAMORPH (Molecular devices).

Atomic force microscopy. The solution of myosin filaments was placed onto a glass coverslip. The samples were imaged by AFM using a NanoWizard III (JPK, Germany) in tapping mode using a very soft probe (tip frequency of 13 kHz). The myosin filament length was measured using METAMORPH (Molecular devices).

Fluorescence microscopy. Samples were imaged within 1–2 min after mixing with an Olympus IX-71 inverted microscope. The sample was excited at 561 nm and 488 nm and the images were recorded simultaneously in two channels using a Dual view Simultaneous Imaging System (Photometrics) with an Andor DV887 EM-CCD camera. Movies overlaying both channels' acquisitions were created using the Metamorph software (Molecular devices). Confocal micrographs were collected using a Leica SP5 laser scanning confocal microscopy system on a DM6000 microscope. The samples were excited at 561 nm and 488 nm.

Data analysis

Mean size of the myosin II cluster. The motor cluster size ℓ was extracted from cryo-TEM and AFM micrographs for [KCl] concentrations of 0.025, 0.05, 0.13, 0.16, and 0.5 M (values correspond to mean ± SD; Fig. S1†). A few tens of myosin filaments were used to extract the mean cluster size for each [KCl]. The dependence of ℓ on the KCl concentration follows a power law: $\ell = 47.5[\mathrm{KCl}]^{-0.8\pm0.04}$. This relationship was further used to calculate the size of the myosin II cluster formed at KCl concentrations of 0.08, 0.15, and 0.17 M (values correspond to mean ± SD; Fig. S1e†).

Mean number of myosin II molecules (two-headed) N_{myo} per motor cluster. The number of myosin II motors (two-headed) per cluster N_{myo} was calculated using the relationship[41] $\frac{\ell - \ell_{bare}}{43} \times 9$, where ℓ is the mean myosin cluster length, $\ell_{bare} = 148$ nm is a head-free region situated in the middle of the bipolar myosin filament (cluster).[42] The ratio 9/43 reflects the organization of myosin molecules within the bipolar filament, *i.e.* 9 two-headed myosin molecules per 43 nm (see ref. 11 and 43 and references therein). Values of N_{myo} are depicted in Fig. S1e† and correspond to mean ± SD.

Force per myosin cluster. The force per cluster $f = p_{att}N_{myo}f_m$, where p_{att} is the fraction of the attached motor in an aggregate, f_m is the force applied by a two-headed myosin molecule 1.4 pN,[44] and N_{myo} is the number of two-headed myosin molecules per cluster.

Image analysis (fluorescence imaging). Myosin II motor clusters were identified, characterized and followed using the well known protocol of Crocker and Grier[45] implemented in the MATLAB software (MathWorks). In this algorithm each motor cluster in an image is assigned a position (x and y coordinates) and a brightness (sum of the intensity of pixels in a window around the motor cluster). Motor clusters in consecutive snapshots are linked using the least squares method.[45] Each identified motor cluster was then assigned a life time (Lt), *i.e.* the time from when it appeared in the field of view until it left it by one of three processes: it was absorbed by another cluster, or the movie ended, or it moved out of focus. In order to study network evolution we studied motor clusters that stayed in the field of view for at least 10 seconds (~100 frames).

The *number of motors* was extracted by counting the number of clusters identified in each snapshot.

Brightness histograms: by grouping the motors according to their lifetimes we were able to calculate the brightness distribution of each group.

Correlation between brightness and lifetime: at each time step the brightness of all motors was normalized to the lowest brightness measured at that time step in order to cancel out differences of illumination and focus between different snapshots and different experiments. The lifetime of the motor clusters was then correlated with their normalized brightness in a specific snapshot, resulting in a single correlation coefficient. This process was repeated for all snapshots to illustrate the change in correlation as a function of time.

Mean square displacement: the mean squared displacement (MSD) of the motor clusters was calculated using their extracted trajectories, according to:

$$\mathrm{MSD}_{\hat{x}}(\tau) = \langle \Delta x^2(\tau) \rangle - \langle \Delta x(\tau) \rangle^2$$

where τ is the lag time and averages are calculated over the ensemble of motor clusters.

The *radius of gyration* R_g of motor motion was calculated according to: $R_g = \sqrt{\frac{1}{\mathrm{Lt}} \sum \left((x - \bar{x})^2 + (y - \bar{y})^2 \right)}$ where Lt is the motor cluster lifetime and $\bar{x}$, $\bar{y}$ is its average location.

D_{rr} and D_{tt}: correlated motion of motor clusters was calculated as is commonly done in two-point microrheology.[46] In this method the correlated motion is decomposed to correlations in the direction connecting the two clusters $\hat{r}$ and the direction perpendicular to it $\hat{t}$. At a given time and lag time each particle moves by:

$$\Delta r^i_{\alpha,\beta}(t,\tau) = r^i_{\alpha,\beta}(t + \tau) - r^i_{\alpha,\beta}(t)$$

where α and β labels represent coordinates, i is the particle number, t is time, and τ is the lag time. Averaging over the ensemble of motor clusters (~200 in our analysis) at a given distance, $r = R^{ij}(t)$, at a given time lag τ, we have:

$$D_{\alpha\beta}(r,t,\tau) = \langle \Delta r^i_\alpha(t,\tau) \Delta r^j_\beta(t,\tau) \delta(r - R^{ij}(t)) \rangle_{i \neq j,t}$$

To increase our sample statistics at each time, t_0, we average over $T = 50$ frames of data:

$$D_{\alpha\beta}(r, t_0, \tau) = \frac{1}{T} \int_{t_0}^{t_0+T} D_{\alpha\beta}(r, t, \tau)\, \mathrm{d}t$$

We then look at the correlated motion at the constant lag time τ as a function of inter-cluster distance, r, at different stages of the experiment, t_0.

Mesh size was measured directly from the actin images using Metamorph (Molecular devices). The mesh size was obtained by measuring the size of the "holes" in the network. For a network undergoing massive coarse graining and disruption, temporal changes in the network mesh size were measured until massive disruption or contraction started.

Distance between motor clusters ξ of the network shown in Fig. 2 was measured directly from the fluorescent images using Metamorph (Molecular devices) ~4 min after mixing (Fig. 2b), by determining the inter-cluster distance of 125 cluster pairs positioned along the network bundles. We find $\xi = 25 \pm 9$ μm (mean ± SD).

We also estimate the inter-cluster distance ξ_{calc} from the ratio ([A]/370)/[M]/N_{myo} [μm], where [A]/370 is the total length of actin filaments available for myosin II attachment and 370 is the number of actin subunits per μm filament. This calculation assumes that every motor cluster intercalated inside a network bundle can interact with any of the filaments residing inside that bundle. This value reflects a *lower* limit for ξ, as it also assumes that *all* the motors are embedded inside the network (with no motor clusters left in solution) and that the system starts the coarse graining process only after its formation is completed. The assumption that the majority of the motor clusters get embedded within the network at its very initial stages of formation is probably exaggerated, yet, it seems to be a plausible assumption when working at low KCl contents (*e.g.*, 0.025 M). Note that under these conditions the concentration of clusters is very low, typically tenths of nM. For instance, at A/M = 150 and $N_{myo} = 144$ (cluster concentration [M]/N_{myo} = 0.086 nM), we get $\xi_{calc} = 58 \pm 14$ μm, which is of the same order of magnitude as the measured one (see Fig. 2b), only smaller implying that the network had time to coarsen.

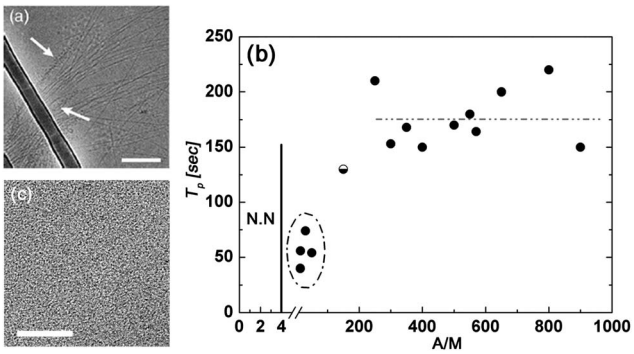

Fig. 1 (a) Cryo-TEM image of myosin II clusters attached to or embedded within actin bundles (white arrows). Conditions: [A] = 2 μM, [KCl] = 0.13 M. Bar: 200 nm. (b) Initial time of formation of visible objects (actin bundles), T_p, as a function of myosin II concentration. At low myosin concentrations network formation takes approximately 175 s. As the myosin concentration exceeds A/M = 200 network formation accelerates up. At A/M = 10–50 networks form already after ~50 s. The dashed-ellipse marks the regime of nucleation enhancement activity by the myosin II cluster. The half hollow half filled circle marks an intermediate behavior regime of T_p ([A]/[M] = 150). For [A]/[M] < 4 bundles do not form and the system consists essentially of individual filaments (N.N describes no-network formation). Conditions: [A] = 5 μM, [A]/[F] = 18, [KCl] = 0.025 M, $MgCl_2$ = 1 mM, and [ATP] = 1 mM. (c) Cryo-TEM image of myosin II at [A]/[M] = 0.333. The black dots are actin monomers. Conditions: [A] = 2 μM, [KCl] = 0.13 M. Bar: 200 nm.

Results and discussion

In vitro models of cytoskeletal networks follow several stages of evolution: nucleation, formation, reorganization and occasionally contraction and rupture. As one of the active ingredients in this system, myosin motor clusters play a major role in all of these processes. In the following we will describe the part myosin II plays in these various processes. For this purpose we have examined a set of five control parameters governing the properties of our reconstituted networks: myosin II ([M]), G-actin ([A]), fascin – passive crosslinker ([F]), ATP, and KCl ([KCl]) concentrations. We found that motors' concentration and KCl concentration affect the network morphology and dynamics the most, where the KCl concentration controls the cluster size ℓ and thus the number of myosin II molecules N_{myo} per cluster.

It has been shown previously[47] that fascin promotes actin polymerization by creating a nucleus from which the actin filaments elongate and subsequently bundle. The capacity of myosin II clusters to intercalate within the growing actin bundles and interact with numerous filaments (Fig. 1a) is expected to enhance the nucleation efficiency, in proportion to the amount of added motor. In order to study the combined effect of fascin and myosin on network nucleation we performed a set of experiments with constant actin and fascin concentration ([A] = 5 μM, [A]/[F] = A/F = 18), changing only the amount of myosin motors, *i.e.* the concentration ratios A/M and F/M. In Fig. 1b the time to create a fluorescently observable network feature, T_p, is plotted as a function of A/M. Clearly, at low myosin concentrations (A/M > 200) network formation does not depend on the myosin concentration and the bundling process is dominated by fascin (T_p is constant and equals 175 s). As the myosin concentration exceeds A/M = 200 network formation is accelerated. Raising the concentration of myosin to A/M = 10–50 speeds up the process by 3-fold ($T_p \sim 50$ s). This implies that already at a ratio of 1 to 400 of active to passive cross-linkers (myosin clusters to fascin molecules, ([F]/([M]/N_{myo})), myosin dominates as a nucleating agent. At very high myosin concentrations (A/M < 4) bundles do not form and the system consists essentially of individual actin filaments (data not shown), in accord with previous results.[12,33] A further increase in motor concentration to A/M = 1/3 leads to the depolymerization of the actin filaments (Fig. 1c). Our conclusion, therefore, is that fascin and myosin II clusters function as co-nucleators of actomyosin networks, where the addition of motor clusters greatly facilitates this process, as manifested in the acceleration of network formation. Interestingly, if motors are introduced in their monomer form network formation is prolonged (data not shown), supporting our hypothesis that the acceleration of network formation is related to the functionality of myosin clusters as internal active crosslinks.

After the initial stage of network polymerization, the system starts reorganizing. From this stage on the function of myosin II motors turns from a network nucleating agent into a network

reorganizing agent. We followed network dynamics by labeling both actin (red) and myosin (green) and imaging them simultaneously (Movie S1†). Myosin assisted self-organization of actin networks in our experimental conditions is initiated almost instantaneously. At first we observed only individual motor clusters as the actin bundles are too fine to detect (Fig. 2a). The motor positions trace the outline of the network structure that appears at later times (Figs. 2b and c). At this stage (Fig. 2b, ~4 min after mixing), the measured inter-cluster distance is $\xi \sim 25 \pm 9$ μm and is in accord with the calculated one suggesting that the majority of the motor clusters are embedded within the network structure (see details in Materials and methods). We tracked the myosin motor clusters using conventional image analysis techniques[45] and find that the cluster motion along those traces is correlated from the onset of the experiment, as shown in Figs. 2d–f. These figures depict the correlated motion of pairs of motor clusters in the direction connecting the center of the motors D_{rr} and perpendicular to it D_{tt}. The fact that a clear signal is observed by analyzing the motion of an ensemble of only 200 motor clusters implies that the correlation between motor clusters' motion is strong. Correlations between the motors exist even at the shortest time scales, in accord with the fact that the motors are embedded inside the network during network formation. At short distances motor motion reflects the reorganization processes occurring in the actin network. Such processes can involve motors moving in the same direction with $D_{rr} > 0$, or motors moving in opposite directions with $D_{rr} < 0$ (Figs. 2d and e). At large distances motion correlations reflect the stiffness and connectivity of the network, hence correlations are essentially positive, and increase with network time of evolution (compare D_{rr} of $r > 50$ μm in Figs. 2d–f). The measured correlation is much more pronounced than in a thermally driven equilibrium gel (data not shown), in which such little statistics would not result in a significant signal. Although in Fig. 2c the system seems to have reached mechanical equilibrium, at some point that system underwent rapid macroscopic contraction (Movies S2 and S3†).

The embedded motors which act as force dipoles inside the network lead with time to network coarse graining, *i.e.* coalescence of fine network features into larger structures. The applied forces can induce the relative sliding and tearing of bundles (Movie S4†), bundle pulling (Movies S5 and S6†), wrapping and severing (Movie S7†), and buckling (Movies S6 and S8†).[34,35] The dynamics and extent of network coarse graining depend on the properties of the motor clusters, notably on their size ℓ and concentration. While the cluster size influences the mean force f that a motor aggregate can generate, the clusters' concentration controls the density of force centers ξ^{-1}, where ξ is the mean distance between them (see Materials and methods).

We estimated the force per cluster by measuring the KCl dependence of motor cluster size ℓ (Fig. 3; see also Materials and methods for details). For that we used high resolution cryo-transmission electron microscopy (cryo-TEM) and atomic force microscopy (AFM) (Fig. S1†). We find that the mean cluster size ℓ decreases with KCl concentration as $\ell \sim [\mathrm{KCl}]^{-0.8}$ (inset, Fig. 3). We use ℓ to estimate N_{myo}, the mean number of myosin II molecules per cluster (detailed in Materials and methods; Fig. S1e†) and the typical force f a motor aggregate can generate. For that we estimate the fraction of attached motor per cluster p_{att} (sometimes also referred to as the 'duty ratio', d). We extract

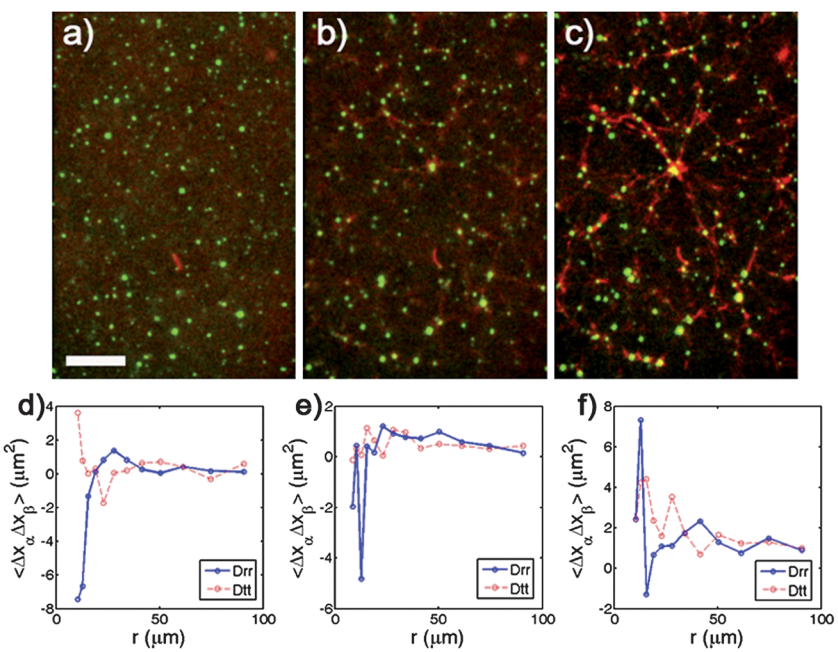

Fig. 2 Snapshots of the evolution of an actin–myosin–fascin network as a function of time, at short times (red – actin, green – myosin); (a) 183 s, (b) 250 s, and (c) 284 s after mixing. Conditions: [A] = 5 μM, [A]/[M] = 150, [A]/[F] = 18, [KCl] = 0.025 M, $MgCl_2$ = 1 mM, and [ATP] = 1 mM. Bar is 100 μm. (d–f) Correlated motion of pairs of motor clusters in the direction connecting the center of the motors D_{rr} and perpendicular to it D_{tt} as a function of inter-cluster distance, r, at different stages of the experiment: (d) 150 s, (e) 217 s, and (f) 250 s.

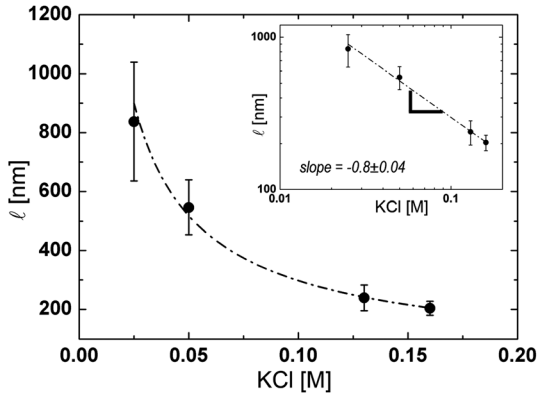

Fig. 3 Mean motor cluster size ℓ as a function of [KCl] exhibits a power law dependence of $\sim[\mathrm{KCl}]^{-0.8\pm0.04}$ as extracted from the fit of the log–log plot (inset). Values correspond to mean ± SD.

this number from the smallest cluster that gives rise to actomyosin network reorganization. In our experiments networks form up to 0.15 M KCl concentration (see below). This means that small clusters composed of 14 double-headed myosin II molecules (Fig. S1e†) move processively and are capable of acting as active cross-linkers (*i.e.*, at *least* 2 among the 14 motor molecules are attached to actin at a given instant, giving a fraction of attached motors of $p_{\mathrm{att}} = 0.15$). This sets a lower limit estimation for motor cluster size to induce self-organization. This also suggests that embedded myosin II clusters have a higher duty ratio d than unconfined motors. $P_{\mathrm{att}} = 0.15$ is typically 4-fold larger than the characteristic duty ratio measured under unloaded conditions on individual actin filaments ($P_{\mathrm{att}} = 0.04$).[48] Note that for KCl concentrations below 0.15 M, $p_{\mathrm{att}} = 0.15$ corresponds to a minimum estimation of the fraction of attached motors; in fact, we expect p_{att} to increase gradually with the decrease in the solution ionic strength.[49] Yet, because we do not know the actual value of p_{att} for each KCl concentration, we use $p_{\mathrm{att}} = 0.15$ to calculate the (minimal) force generated per cluster. Under these conditions, the forces range from 3.0 ± 0.3 pN to 30 ± 7 pN for N_{myo} ranging from 14 ± 2 (at [KCl] = 0.15 M) to 144 ± 34 (at [KCl] = 0.025 M), respectively. Using N_{myo} we calculate the concentration of motor clusters ($[\mathrm{M}]/N_{\mathrm{myo}}$) which serve as a means to estimate the density of force points in the network and their density per unit length ξ_{calc}^{-1} (here we assume that the majority of the motors are embedded in the network, which appears to be a plausible assumption; see Materials and methods for details). Generally, we find that for large clusters (N_{myo} = 84–144), the system is highly dynamic and undergoes a high degree of coarse graining. Under these conditions the system can end up either in full contraction (low and intermediate $[\mathrm{M}]/N_{\mathrm{myo}}$ and large N_{myo}, see Movies S2 and S3†) or disruption (high $[\mathrm{M}]/N_{\mathrm{myo}}$ and large N_{myo}, see Movies S4 and S9†).

In contrast, for small and intermediate motor clusters the system undergoes much less rearrangement and forms mechanically stable tensile networks (see the '3D-phase diagram' below) with a typical mesh size of a few microns (Fig. S2†).[33] Inspection of the conditions for which tensile networks form shows that the motor clusters range between $N_{\mathrm{myo}} = 14 \pm 2$ (0.15 M KCl) and $N_{\mathrm{myo}} = 44 \pm 5$ (0.08 M KCl) and apply relatively small forces ranging between 3.0 ± 0.3 pN and 9.2 ± 1.0 pN, respectively. Also, tensile networks form at relatively high motor contents $18 \leq [\mathrm{A}]/[\mathrm{M}] \leq 40$ (and fascin $7 \leq [\mathrm{A}]/[\mathrm{F}] \leq 40$) thereby setting the inter-cluster distance at the sub-micron to micron scale, $\xi_{\mathrm{calc}} = 0.4$–$1.8$ μm (see details in Materials and methods). This distance is comparable to the size of the myosin clusters (Fig. S1e†), implying that the clusters are densely packed and homogeneously distributed inside the network. Under these conditions mechanically stable network structures are formed exhibiting little dynamics and virtually no reorganization.

In order to study the dynamics of actomyosin reorganization, we focus on networks consisting of big motor clusters (N_{myo} = 144, 0.025 M KCl), since they exhibit highly dynamic structures and undergo various degrees of coarse graining, depending on the amount of myosin II added (A/M). Under these salt conditions the motor clusters are completely processive, and are never observed to detach from the actin network. We tracked the myosin clusters and measured the lifetime of each cluster, Lt, from its initial sighting to its coalescence with a (nearby) cluster. Motor cluster dynamics vary significantly and can be divided according to their mobility and lifetime (Fig. 4, [A]/[M] = 150 and $\xi_{\mathrm{calc}} \approx 58$ μm). We use the radius of gyration of a cluster's trajectory, R_g, to characterize the range of their motion (Fig. S3†). On average, motors undergo seemingly random motion; we discriminate between relatively confined motors and relatively dynamic ones. Cluster analysis from the plot of R_g as a function of lifetime Lt (Fig. 4a) reveals several distinct motor cluster behaviors; long living motors which are confined (dashed red oval), mobile motors with intermediate lifetimes (dash-dotted cyan oval), short lived mobile motors (dotted magenta oval), and static motors (green oval – these probably represent stuck motors to the glass surface). The different classes can be related to the dynamics of coarse graining. For example, the trajectory of a confined, long lived, motor is depicted in the center of the inset of Fig. 4a (magenta trajectory

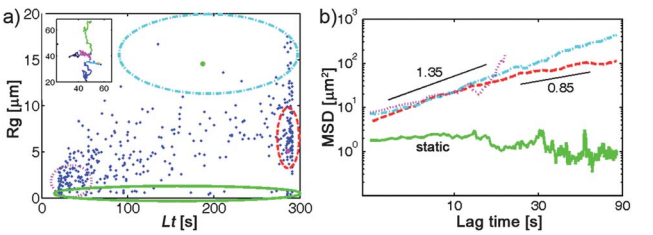

Fig. 4 Mobility analysis of motor clusters' motion. Types of motor mobilities include: long duration and confined (dashed red oval), mobile with intermediate duration (dash-dotted cyan oval), short duration and mobile (dotted magenta oval), and static (green oval). (a) Radius of gyration of motor cluster motion as a function of motor cluster lifetime. The inset shows trajectories of several motor clusters, a pulling motor (magenta) which is highlighted in the main figure by a magenta dot, and a motor cluster it is pulling (green) highlighted in the main figure by a green dot. (b) The average MSD of motor clusters from the different mobility groups. At short times mobile motors exhibit super-diffusion (slope ~1.35), which changes gradually to sub-diffusion (slope ~0.85) for confined motors. Conditions: [A] = 5 μM, [A]/[M] = 150, [A]/[F] = 18, [KCl] = 0.025 M, $MgCl_2$ = 1 mM, and [ATP] = 1 mM.

in the inset and magenta highlight in the figure). The trajectories of other motors moving towards this relatively confined motor are depicted as well. See for example the trajectory (green) of a mobile motor with an intermediate lifetime marked in green in Fig. 4a; its attraction towards the confined motor is reminiscent of a bundle pulling process (Movie S10† – upside down view of the inset in Fig. 4a). The type of motion associated with these motor groups is characterized by their mean square displacement, MSD (Fig. 4b). All mobile motors exhibit super-diffusion (slope >1) at short time scales. However, a transition into sub-diffusion (slope <1) is observed for confined motors (*i.e.* pulling ones).

At [A]/[M] = 150 (Figs. 2 and 4) the network does not change its structure significantly during the early evolution stages before contracting. However, at larger myosin content ([A]/[M] = 10 for which $\xi_{calc} \approx 4$ μm) dramatic rearrangements are observed already from the very beginning of network evolution (see also Fig. S4†). Specifically, we concentrated on a series of experiments in which the [A]/[M] ranges from 10 to 650. At high myosin concentrations the evolution of the network involves significant multi-scale reorganization[34,50,51] which ends by its complete disruption ([A]/[M] = 10,15). The extent of coarse graining decreases gradually with the decrease in myosin concentration. At low myosin concentrations ([A]/[M] = 400–650) network reorganization is barely observed. Except for networks containing high myosin concentrations ([A]/[M] = 10,15), all networks undergo macroscopic contraction at some point.

In order to quantify the extent of coarsening and its evolution with time we measured the lifetime of each cluster, Lt. In addition, we measured the motor cluster brightness, Br, and the number of clusters, *N*, as a function of time. It is not clear whether during network evolution myosin clusters can continue to self-assemble into larger clusters, or whether they are simply pulled together. We do not discriminate between these two scenarios, but assume that either way, the total force applied by a motor aggregate is related to the total number of motors in that assembly. We further assume that the total brightness of a myosin aggregate is directly related to the total number of motors in that assembly, as a constant percentage of myosin monomers are fluorescently labeled. In Fig. 5a we compare several systems ranging in their coarsening and reorganization extent. The process of reorganization is quantified using three observables: the number of identified motor clusters, the average motor size (brightness), and the correlation between the motor cluster size and motor cluster lifetime. Quantitatively the relationship between the cluster brightness at time *t* and its lifetime can be characterized by their correlation coefficient:

$$\mathrm{Corr}\,(t) = \frac{\langle \mathrm{Br}_{i,t}\mathrm{Lt}_i \rangle}{\langle \mathrm{Br}_t \rangle \langle \mathrm{Lt} \rangle}$$

where $\mathrm{Br}_{i,t}$ is the brightness of motor cluster *i* at time *t*, Lt_i is its lifetime, and the brackets denote an average over all motor clusters.

In the process of reorganization we expect the number of motor clusters to decrease in time as motors coalesce (Fig. 5a $t >$ 100 s), the average motor cluster brightness to increase (Fig. 5b, inset), and the correlation of size to lifetime at the end of the reorganization process, $\mathrm{Corr}_\infty = \mathrm{Corr}(t \to \infty)$, to increase with the extent of reorganization (Fig. 5d). This process is further confirmed by the fact that longevity implies higher brightness (Fig. 5b). Interestingly we find that an additional stage of reorganization is observed at high myosin content, where the

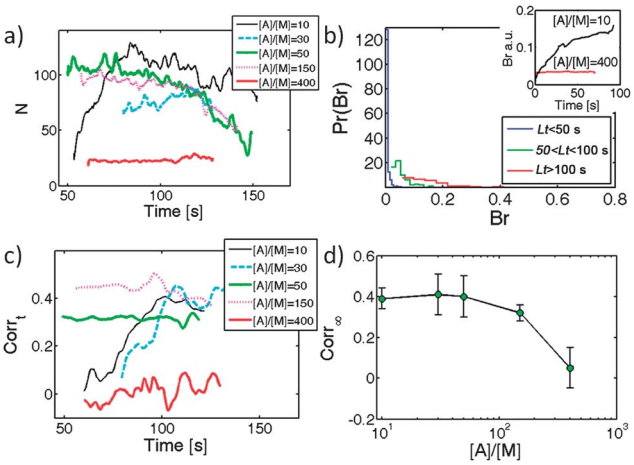

Fig. 5 Network evolution as a function of [A]/[M]. (a) Number of motors as a function of time. (b) Motor cluster brightness distributions for motors with different lifetimes, Lt; the inset shows average cluster brightness as a function of evolution time for high ([A]/[M] = 10) and low ([A]/[M] = 400) myosin concentrations. (c) Correlation between motor cluster brightness at a given time, Corr_t, and its lifetime (see details in the text). (d) Long time correlation, Corr_∞, as a function of [A]/[M]. Values correspond to mean ± SD. Conditions: [A] = 5 μM, [A]/[F] = 18, [KCl] = 0.025 M, $MgCl_2$ = 1 mM, and [ATP] = 1 mM.

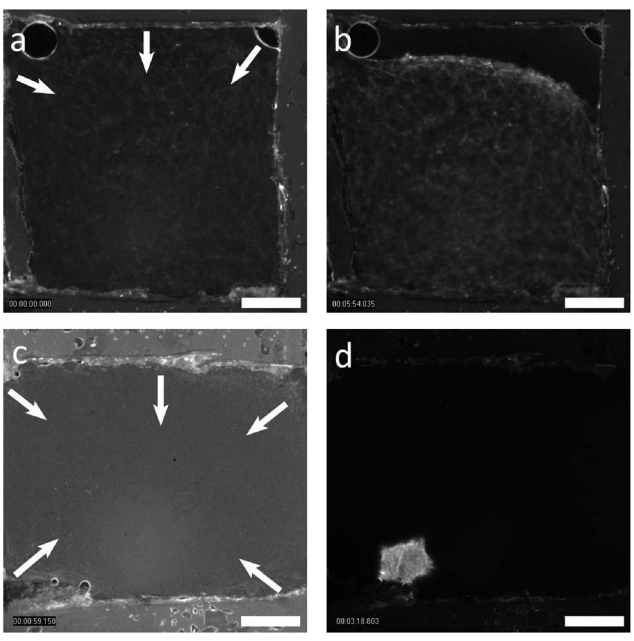

Fig. 6 Embedded *vs.* un-embedded motors in actomyosin network polymerization, contractility. Condition: [A] = 5 μM, [A]/[M] = 350, [A]/[F] = 18, [KCl] = 0.025 M, $MgCl_2$ = 1 mM, and [ATP] = 1 mM. (a and b) Polymerization of a network of actin/fascin bundles precedes motor addition, resulting in marginal contractility; initial (a) and final (b) stages. (c and d) Similar systems to those in (a and b) but the motor clusters are embedded within the network structure from its very initial stages of formation, resulting in prominent contractility; initial (c) and final (d) stages. The arrows mark the direction of contractility. Bars: 550 μm.

number of motor clusters increases at initial stages of reorganization (Fig. 5a A/M = 10,30) coupled with an increase in the correlation of size and lifetime (Fig. 5c A/M = 10,30). This suggests that the motors which assimilate other motors do not necessarily start as the largest motors. At low myosin concentrations little reorganization is observed confirming the role of myosin as the *reorganizer* agent in actomyosin networks.

Actomyosin networks can form either mechanically stable structures (tensile networks) that do not undergo further reorganization with time, or the dynamic structures described above. The reorganization of the dynamic actomyosin networks is always followed by one of two processes: contraction or disruption. If the myosin motors are not embedded in the network from the start, but are added after its initial formation, the whole network evolution is suppressed (Fig. 6).

To reflect the prominent effect of the motor cluster size and concentration on the final morphology of an actomyosin network, a 3D phase diagram of networks' final states is plotted as a function of ℓ, $[M]/N_{myo}$, and actin concentration [A] for two different [A]/[F] (Fig. 7). In the absence of motors we observe the formation of actin/fascin bundles (Fig. 7b), which do not undergo further reorganization, indicating that network coarsening is associated with motor activity. For large clusters (N_{myo} = 144, [KCl] = 0.025 M) and high motor concentrations the network

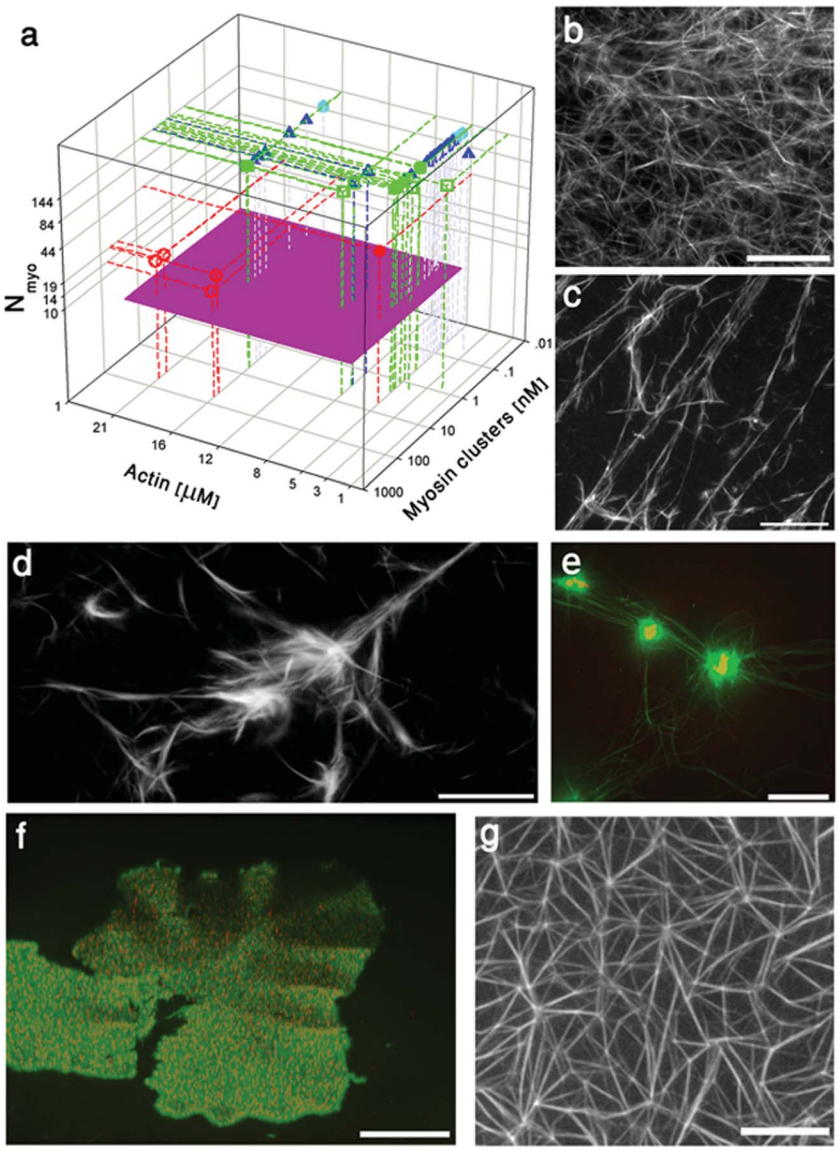

Fig. 7 (a) 3D phase diagram of network final states *vs.* ℓ, $[M]/N_{myo}$ and actin concentration [A] for two different [A]/[F]. Red circles, cyan hexagons, blue triangles, and green rectangles correspond to 'tensile', 'entangled', 'contractile', and disintegrated networks, respectively. Filled and hollow symbols correspond to networks formed at [A]/[F] = 18 and 7, respectively. (b–g) Optical fluorescence imaging of actomyosin networks formed at different system compositions. (b) Entangled actin/fascin network form in the absence of motors. (e and f) For large clusters, networks can undergo massive coarse graining and disruption ending-up either in (c) tensile fibers, (d) patches, or (e) aster-like structures where myosin II motors accumulate at the center (actin – green and myosin – red). (f) Intermediate motor content and large cluster sizes induce macroscopic contraction (green - actin and red - myosin II). (g) Tensile networks form in the presence of intermediate and small clusters and high motor contents. Conditions: 0.025 M (c–f), 0.05 M (b), 0.13 M KCl (g). [G-actin]: 20 μM (g), 16 μM (d), 8 μM (c), 5 μM (e and f), and 4 μM (b). [A]/[M]: 0 (b), 9 (c), 18 (d and g), 300 (e), and 400 (f). [A]/[F]: 7 (c, d and g), 18 (e and f), and 20 (b). The concentrations of Mg-ATP and $MgCl_2$ are equal to 1 mM. Bars: 200 μm (c), 40 μm (b), 50 μm (d), 20 μm (e and g), and 300 μm (f).

disintegrates into either tensile fibers (Fig. 7c), patches (Fig. 7d; Movie S9†), or aster-like structures (Fig. 7e), where the final structure type depends on both [A] and [A]/[F]. At intermediate myosin concentrations ($30 \leq [A]/[M] \leq 1000$), we observe networks ending up in macroscopic contraction (Fig. 7f; Movies S2 and S3†). At small and intermediate motor clusters (ranging between $N_{myo} = 14 \pm 2$ and 44 ± 5 for 0.08–0.15 M KCl) and motor concentrations of $18 \leq [A]/[M] \leq 40$, the system forms a mechanically stable tensile network (Fig. 7g). Active networks do not form at concentrations equal to or higher than 0.17 M KCl (Figs. 7a and S2†) suggesting that the clusters are not processive and cannot act as active cross-linkers (*i.e.*, less than two motors are attached at once). Indeed, under these salt conditions, $N_{myo} = 10$ (Fig. S1e†) and $p_{att} < 0.15$,[49] which gives a mean number of attached motors smaller than two. Finally, for $[A]/[M] \leq 3$ the severing and depolymerization activity of myosin II dominates, preventing the assembly of actin bundles and formation of actomyosin networks, in accord with our previous results.[33]

Conclusions

The myosin II motor stands out for the multiple roles it plays in cytoskeleton self-assembly and reorganization in contrast to other motors such as kinesin. Here we present evidence for myosin II functionality ranging from a network *co-nucleator*, through an active *organizer* of the network structure, to a *severing* and *regulating agent* of actin turnover. We do not know of any other motors in cells that have such a diversity of functions. The vast range of myosin II functions probably has to do with the properties of the individual myosin II molecules (highly non-processive), and their ability to form motor clusters that can be internalized within the network structure, where they can actively build tension into the existing network.[52]

In our *in vitro* experiments, we show that during the initial process of network formation the motors become embedded within the network and take part in its formation. Myosin II motors enhance the nucleation of actin filaments/bundles in a concentration dependent manner, in the presence of fascin. This process is further enhanced when myosin II is in the form of motor clusters. The motors that are embedded within the network are acting as internal active cross-links that apply pinching forces at the molecular level. As a result of the strong confinement the motor clusters exhibit high processivity ($p_{att} \geq 0.15$, *i.e.*, more than 4-fold higher in comparison to unconfined conditions[48]), rendering even small clusters of 14 myosin molecules efficient active cross-linkers. This enhanced processivity may result from several reasons: (i) *confinement effects* – the confinement can *effectively* increase individual motors and motor cluster processivity by prohibiting their escape and increasing their chance to rebind, after terminating their ATPase cycle and detaching from an actin filament. (ii) *Application of resistive loads* – previous studies have demonstrated that resistive loads increase myosin II motors' duty ratio to favor tension maintenance.[53,54] In our experimental system both effects could act simultaneously. The motor clusters embedded within the actin network are expected to be subjected to resistive loads and large confinements, and therefore to have an enhanced duty ratio and processivity.

The motor clusters can vary in size between 14 and 144 myosin II molecules and apply forces ranging from several to tens of pN (at least), depending on the KCl concentration. The dynamics of the system is highly dependent on the size and concentration of the motor clusters, as both determine the distribution and magnitude of force centers in the networks. Homogeneous and dense distribution of force points (which apply forces up to 10 pN) lead to the formation of tensile networks that are mechanically stable, in accord with our previous results using intermediate sized clusters.[33]

When the motor clusters apply large forces (tens of pN and more) and when the distribution of these force centers is sparse (leading to local force in-homogeneities), the system becomes much less stable and can undergo enhanced coarsening, depending on the concentration of the motor clusters. Under these conditions the system is highly dynamic and correlation in the movement of motor cluster pairs is found. Generally we find that big motor clusters pull nearby small motor clusters, leading to their active transport, and to their coalescence. We characterized this process by analyzing the correlated motion of pairs of motor clusters in the direction connecting the center of the motors D_{rr} and perpendicular to it D_{tt}. We show that there exist correlations between the motors even at the shortest time scales, where D_{rr} exhibits both anti-correlation (motors are pulled one towards the other, hence $D_{rr} < 0$) and positive correlations (motors move in the same direction with $D_{rr} > 0$) at short distances. As time evolves these pulling effects lead to multi-stage network coarsening, the extent of which depends on the motor cluster concentration. Network coarsening is not unique to our system, and seems to be an inherent property of actomyosin networks.[34,50,51]

At longer time scales the stresses building-up in these networks lead to complex dynamics and can drive their contraction[55,56] and rupture, depending on the motor concentration and cluster size. Contractility seems to be a generic property of myosin II motor/filament systems, and has to do with the fact that a motor within a motor-aggregate can interact with multiple filaments simultaneously. Those filaments, which can be of opposite orientations/polarity, lead to the formation of 'contractile units' within the network. Global contraction is induced by the collective action of those randomly distributed contractile units, as long as they apply sufficiently large forces ($f \geq$ tens of pN, 0.025 M KCl) and are sparsely distributed ($30 \leq [A]/[M] \leq 1000$). If the clusters' density gets too large ($A/M \leq 15$) the network will disrupt instead of contracting, whereas at intermediate A/M both phenomena can occur. The formation of contractile elements was also used to explain the contractility of reconstituted actomyosin bundles (1D structure) *in vitro*.[57] Kruse and Jülicher predicted theoretically the spontaneous contraction of bundles of polar filaments by molecular motors.[58] To conclude, myosin II motors are unique motors that function as complex machines that can perform a diversity of tasks. While myosin's roles in reorganization and disassembly of networks were highlighted before in various studies, the importance of myosin II in the assembly of actomyosin

networks could be more profound than previously thought. We have shown that myosin II activity in the early stages of network formation regulates the nature of the assembled network and facilitates its formation. The multi-tasking function of myosin II motors is an intrinsic property of these motors and is also observed *in vivo*. In cells myosin II motors perform all the type of functions that we observed in our reconstituted systems, including assembly, reorganization, and disassembly. For instance, they participate in contractile ring and stress fiber assembly,[59,60] in wound healing and gastrulation by actively remodeling actomyosin networks,[7–10] and finally, they control actin turnover and network disassembly.[13–17] By controlling the activity and concentration of the motor clusters, the cell can control and tune the relevant myosin II function necessitated for a given process.

Acknowledgements

We would like to thank Tom Pollard, Nir Gov, and Barak Gilboa for careful reading of the manuscript and useful comments. A.B.-G. thanks the Israel Science Foundation (grant #1534/10) and DFG (grant #KR 3430/3-1) for financial support. A.B.-G. is grateful to Yale Goldman for kindly providing the RLC mutant construct. Y.R. thanks the CEC under a Marie Curie Reintegration Grant (#PIRG04-GA-2008-239378) for financial support.

References

1 Y. L. Wang, *J. Cell Biol.*, 1985, **101**, 597–602.
2 J. Howard, *Mechanics of Motor Proteins and the Cytoskeleton*, Sinauer Associates, Sunderland, 2001.
3 M. Vicente-Manzanares, X. Ma, R. S. Adelstein and A. R. Horwitz, *Nat. Rev. Mol. Cell Biol.*, 2009, **10**, 778–790, DOI: 10.1038/nrm2786.
4 J. Q. Wu and T. D. Pollard, *Science*, 2005, **310**, 310–314, DOI: 10.1126/science.1113230.
5 A. Carvalho, A. Desai and K. Oegema, *Cell*, 2009, **137**, 926–937, DOI: 10.1016/j.cell.2009.03.021.
6 X. Ma, M. Kovacs, M. A. Conti, A. Wang, Y. Zhang, J. R. Sellers and R. S. Adelstein, *Proc. Natl. Acad. Sci. U. S. A.*, 2012, **109**, 4509–4514, DOI: 10.1073/pnas.1116268109.
7 A. C. Martin, *Dev. Biol.*, 2010, **341**, 114–125, DOI: 10.1016/j.ydbio.2009.10.031.
8 T. Lecuit, P. F. Lenne and E. Munro, *Annu. Rev. Cell Dev. Biol.*, 2011, **27**, 157–184, DOI: 10.1146/annurev-cellbio-100109-104027.
9 M. Mayer, M. Depken, J. S. Bois, F. Julicher and S. W. Grill, *Nature*, 2010, **467**, 617–621, DOI: 10.1038/nature09376.
10 S. N. Hird and J. G. White, *J. Cell Biol.*, 1993, **121**, 1343–1355.
11 M. Stewart and R. W. Kensler, *J. Mol. Biol.*, 1986, **192**, 831–851.
12 L. Haviv, D. Gillo, F. Backouche and A. Bernheim-Groswasser, *J. Mol. Biol.*, 2008, **375**, 325–330, DOI: 10.1016/j.jmb.2007.09.066.
13 C. A. Wilson, M. A. Tsuchida, G. M. Allen, E. L. Barnhart, K. T. Applegate, P. T. Yam, L. Ji, K. Keren, G. Danuser and J. A. Theriot, *Nature*, 2010, **465**, 373–377, DOI: 10.1038/nature08994.
14 R. J. Pelham and F. Chang, *Nature*, 2002, **419**, 82–86, DOI: 10.1038/nature00999.
15 M. Guha, M. Zhou and Y. L. Wang, *Curr. Biol.*, 2005, **15**, 732–736, DOI: 10.1016/j.cub.2005.03.042.
16 K. Murthy and P. Wadsworth, *Curr. Biol.*, 2005, **15**, 724–731, DOI: 10.1016/j.cub.2005.02.055.
17 D. R. Burgess, *Curr. Biol.*, 2005, **15**, R310–R311, DOI: 10.1016/j.cub.2005.04.008.
18 A. C. Reymann, R. Boujemaa-Paterski, J. L. Martiel, C. Guerin, W. Cao, H. F. Chin, E. M. De La Cruz, M. Thery and L. Blanchoin, *Science*, 2012, **336**, 1310–1314, DOI: 10.1126/science.1221708.
19 T. Surrey, F. Nedelec, S. Leibler and E. Karsenti, *Science*, 2001, **292**, 1167–1171, DOI: 10.1126/science.1059758.
20 F. J. Nedelec, T. Surrey, A. C. Maggs and S. Leibler, *Nature*, 1997, **389**, 305–308, DOI: 10.1038/38532.
21 C. Hentrich and T. Surrey, *J. Cell Biol.*, 2010, **189**, 465–480, DOI: 10.1083/jcb.200910125.
22 R. Urrutia, M. A. McNiven, J. P. Albanesi, D. B. Murphy and B. Kachar, *Proc. Natl. Acad. Sci. U. S. A.*, 1991, **88**, 6701–6705.
23 S. Sankararaman, G. I. Menon and P. B. Kumar, *Phys. Rev. E: Stat., Nonlinear, Soft Matter Phys.*, 2004, **70**, 031905.
24 F. Nédélec and T. Surrey, *C. R. Acad. Sci., Ser. IV: Phys., Astrophys.*, 2001, **2**, 841–847.
25 F. Jülicher, K. Kruse, J. Prost and J. F. Joanny, *Phys. Rep.*, 2007, **449**, 3–28.
26 T. B. Liverpool, *Philos. Trans. R. Soc., A*, 2006, **364**, 3335–3355, DOI: 10.1098/rsta.2006.1897.
27 B. Bassetti, M. Cosentino Lagomarsino and P. Jona, *Eur. Phys. J. B*, 2000, **15**, 483–492, DOI: 10.1007/s100510051150.
28 K. Kruse, J. F. Joanny, F. Julicher, J. Prost and K. Sekimoto, *Phys. Rev. Lett.*, 2004, **92**, 078101.
29 I. S. Aranson and L. S. Tsimring, *Phys. Rev. E: Stat., Nonlinear, Soft Matter Phys.*, 2005, **71**, 050901.
30 F. Ziebert and W. Zimmermann, *Eur. Phys. J. E: Soft Matter Biol. Phys.*, 2005, **18**, 41–54, DOI: 10.1140/epje/i2005-10029-3.
31 H. Y. Lee and M. Kardar, *Phys. Rev. E: Stat., Nonlinear, Soft Matter Phys.*, 2001, **64**, 056113.
32 F. Nedelec, *J. Cell Biol.*, 2002, **158**, 1005–1015, DOI: 10.1083/jcb.200202051.
33 F. Backouche, L. Haviv, D. Groswasser and A. Bernheim-Groswasser, *Phys. Biol.*, 2006, **3**, 264–273, DOI: 10.1088/1478-3975/3/4/004.
34 M. Soares e Silva, M. Depken, B. Stuhrmann, M. Korsten, F. C. MacKintosh and G. H. Koenderink, *Proc. Natl. Acad. Sci. U. S. A.*, 2011, **108**, 9408–9413, DOI: 10.1073/pnas.1016616108.
35 M. P. Murrell and M. L. Gardel, *Proc. Natl. Acad. Sci. U. S. A.*, 2012, **109**, 20820–20825, DOI: 10.1073/pnas.1214753109.
36 M. J. Footer, J. W. Kerssemakers, J. A. Theriot and M. Dogterom, *Proc. Natl. Acad. Sci. U. S. A.*, 2007, **104**, 2181–2186, DOI: 10.1073/pnas.0607052104.
37 S. Ono, Y. Yamakita, S. Yamashiro, P. T. Matsudaira, J. R. Gnarra, T. Obinata and F. Matsumura, *J. Biol. Chem.*, 1997, **272**, 2527–2533.
38 J. A. Spudich and S. Watt, *J. Biol. Chem.*, 1971, **246**, 4866–4871.

39 S. S. Margossian and S. Lowey, *Methods Enzymol.*, 1982, **85**(Pt B), 55–71.

40 M. E. Quinlan, J. N. Forkey and Y. E. Goldman, *Biophys. J.*, 2005, **89**, 1132–1142, DOI: 10.1529/biophysj.104.053496.

41 L. Skubiszak and L. Kowalczyk, *Acta Biochim. Pol.*, 2002, **49**, 829–840.

42 M. E. Cantino, M. W. Chew, P. K. Luther, E. Morris and J. M. Squire, *J. Struct. Biol.*, 2002, **137**, 164–175, DOI: 10.1006/jsbi.2002.4474.

43 R. Craig and J. L. Woodhead, *Curr. Opin. Struct. Biol.*, 2006, **16**, 204–212, DOI: 10.1016/j.sbi.2006.03.006.

44 M. J. Tyska, D. E. Dupuis, W. H. Guilford, J. B. Patlak, G. S. Waller, K. M. Trybus, D. M. Warshaw and S. Lowey, *Proc. Natl. Acad. Sci. U. S. A.*, 1999, **96**, 4402–4407.

45 J. C. Crocker and D. G. Grier, *J. Colloid Interface Sci.*, 1996, **179**, 298–310, DOI: 10.1006/jcis.1996.0217.

46 J. C. Crocker, M. T. Valentine, E. R. Weeks, T. Gisler, P. D. Kaplan, A. G. Yodh and D. A. Weitz, *Phys. Rev. Lett.*, 2000, **85**, 888–891, DOI: 10.1103/PhysRevLett.85.888.

47 L. Haviv, N. Gov, Y. Ideses and A. Bernheim-Groswasser, *Eur. Biophys. J.*, 2008, **37**(4), 447–454.

48 D. E. Harris and D. M. Warshaw, *J. Biol. Chem.*, 1993, **268**, 14764–14768.

49 J. M. Chalovich, L. A. Stein, L. E. Greene and E. Eisenberg, *Biochemistry*, 1984, **23**, 4885–4889.

50 S. Kohler, V. Schaller and A. R. Bausch, *Nat. Mater.*, 2011, **10**, 462–468, DOI: 10.1038/nmat3009.

51 S. Kohler, V. Schaller and A. R. Bausch, *PLoS One*, 2011, **6**, e23798, DOI: 10.1371/journal.pone.0023798.

52 G. H. Koenderink, Z. Dogic, F. Nakamura, P. M. Bendix, F. C. MacKintosh, J. H. Hartwig, T. P. Stossel and D. A. Weitz, *Proc. Natl. Acad. Sci. U. S. A.*, 2009, **106**, 15192–15197, DOI: 10.1073/pnas.0903974106.

53 A. K. Tsaturyan, S. Y. Bershitsky, N. A. Koubassova, M. Fernandez, T. Narayanan and M. A. Ferenczi, *Biophys. J.*, 2011, **101**, 404–410, DOI: 10.1016/j.bpj.2011.06.008.

54 M. Kovacs, K. Thirumurugan, P. J. Knight and J. R. Sellers, *Proc. Natl. Acad. Sci. U. S. A.*, 2007, **104**, 9994–9999, DOI: 10.1073/pnas.0701181104.

55 P. M. Bendix, G. H. Koenderink, D. Cuvelier, Z. Dogic, B. N. Koeleman, W. M. Brieher, C. M. Field, L. Mahadevan and D. A. Weitz, *Biophys. J.*, 2008, **94**, 3126–3136, DOI: 10.1529/biophysj.107.117960.

56 S. Kohler and A. R. Bausch, *PLoS One*, 2012, **7**, e39869, DOI: 10.1371/journal.pone.0039869.

57 T. Thoresen, M. Lenz and M. L. Gardel, *Biophys. J.*, 2011, **100**, 2698–2705.

58 K. Kruse and F. Jülicher, *Phys. Rev. Lett.*, 2000, **85**, 1778–1781.

59 M. Shutova, C. Yang, J. M. Vasiliev and T. Svitkina, *PLoS One*, 2012, **7**, e40814, DOI: 10.1371/journal.pone.0040814.

60 S. Tojkander, G. Gateva, G. Schevzov, P. Hotulainen, P. Naumanen, C. Martin, P. W. Gunning and P. Lappalainen, *Curr. Biol.*, 2011, **21**, 539–550, DOI: 10.1016/j.cub.2011.03.007.